

# Performance Analysis of Cell-free and User-Centric MIMO Networks with Optical Fronthaul and Backhaul Links

Pouya Agheli, Mohammad Javad Emadi, and Hamzeh Beyranvand

Electrical Engineering Department, Amirkabir University of Technology, Tehran, Iran

E-mails: {pouya.agheli, mj.emadi, beyranvand}@aut.ac.ir

## Abstract

Cell-free massive MIMO (CF-mMIMO) network and its variations such the user-centric (UC) one are considered as promising techniques for the forthcoming wireless networks. Also, investigating effects of fronthaul and backhaul links connecting access points (APs) to central processing unit (CPU) is of interest to make it more practical. Thus, we study uplink of CF- and UC-mMIMO networks wherein free space optical fronthauls connect APs to serving aggregation nodes (ANs), and the ANs are connected to the CPU by fiber optic backhauls. To derive the achievable rates, we firstly obtain channel state information by use of uplink pilot transmissions, and then data recovery is performed at the CPU. Moreover, it is assumed that devices at APs and ANs are not ideal and distort the received information/pilot signals. For the CF- and UC-mMIMO setups, optimal transmission power allocations at the users, and optical gain coefficients at the APs and ANs are derived to maximize the achievable sum rates in presence of non-ideal hardware devices by investigating two hardware impairment models. Through numerical results, spectral- and energy-efficiency of the proposed networks are analysed and compared in various circumstances to highlight the effects of resource allocations, hardware impairments, size of the network and weather conditions. It is shown that the performance of the UC-mMIMO network outperforms that of the CF-mMIMO one thanks to the less effective hardware impairments.

## Index Terms

Cell-free massive MIMO, user-centric massive MIMO, free space optical fronthaul, optical fiber backhaul, clipping model, hardware impairment model, uplink achievable data rates.

## I. INTRODUCTION

Key features of novel technologies used in the upcoming wireless networks are to answer the immediate increase of the number of mobile users with high data rates, low latency demands, and energy-efficient communications. The massive multiple-input multiple-output (mMIMO) scheme provides noticeable improvements in spectral efficiency and energy efficiency of the system and applies near-optimal linear processing thanks to the weak law of large numbers [1]. Moreover, it is sufficient to acquire the channel state information (CSI) at the base station, and the user only needs to know the statistical average of the effective channel because of the channel hardening and the uplink and downlink channel reciprocity in the time-division duplex transmission scheme. Thus, there is no pilot transmission overhead in the downlink [2]. Due to the importance of the mMIMO scheme, various modifications of this scheme have been presented in the literature and even deployed [2]–[5]. In particular, the cell-free mMIMO (CF-mMIMO) scheme has been introduced wherein to inherit the advantageous of the distributed and the mMIMO approaches to not only improve spectral efficiency but also to serve users with almost the same quality and high coverage support by applying the straightforward maximum-ratio detection performed at distributed access points (APs) [4]. In the CF-mMIMO network, the APs simultaneously serve all user equipments (UEs) in the same frequency band. Since the access links between APs and UEs are shorter, and the UEs experience almost-surely better channel, the CF-mMIMO network provides higher data rates and wider coverage area compared to the cellular network. For instance, it is shown that the CF-mMIMO network downlink overcomes the small-cell network with about 5-fold and 10-fold improvement in 95%-likely per-user throughput respectively under uncorrelated and correlated shadowing [4].

The CF-mMIMO networks have been investigated from different viewpoints. The max-min power control mechanism for data transmission to ensure uniformly good service within the support area is considered in [4]. Also, the power control mechanisms for pilot transmission to minimize the mean-squared error of the channel estimation is studied in [6], respectively. The user-centric approach in mMIMO network, wherein each user merely connects to its nearby APs, has also been introduced and analyzed in [7]. It is shown that the UC-mMIMO network provides higher per-user data rates in comparison to the CF-mMIMO approach with less fronthaul and backhaul overhead demands [8] and [9]. Moreover, [10] and [11] have analyzed energy efficiency and total power consumption models at APs and backhaul links in the CF-mMIMO network,

where it is assumed that backhaul links are *ideal*. Furthermore, spectral efficiency and energy efficiency expressions have been analyzed for *limited-capacity* fronthaul CF-mMIMO networks in [12] and [13], and the effects of quantization on the network performance have been studied.

On the other hand, optical technologies are mainly employed to deploy fronthaul and backhaul networks by use of the two well-known types of links; optical fiber and free space optical (FSO) links. The optical fiber technology provides high data rates and low path-loss, which comes at the disadvantage of high maintenance, deployment costs, and digging problems. Conversely, the FSO technology still offers large enough data rates with much lower deployment cost, rapid setup time, easy upgrade, flexibility, freedom from spectrum license regulations, and enhanced security. However, it comes at the expense of some drawbacks such as pointing error, the requirement of a line-of-sight (LOS) connection between nodes, and sensitivity to atmosphere conditions including rain, snow, fog, and dust [14]–[16]. To solve the outage problem of the FSO links in adverse atmospheric conditions, the combined radio frequency (RF) and FSO solution is employed for fronthaul and backhaul links, namely hybrid RF/FSO and relay-based cooperation [17]–[23]. Moreover, [24] has studied the joint deployment of RF and FSO fronthaul links in the uplink of a cloud-radio access network (C-RAN), and [25] presents a C-RAN network with RF multiple-access links and hybrid RF/FSO fronthaul links wherein RF-based fronthaul and multiple-access links exploit the same frequency band with the optimized time-division mechanism. Furthermore, in [14], buffer-aided RF/FSO fronthaul links have been utilized to enhance the network performance in adverse weather conditions with the disadvantage of delay. Hassan et. al. [26] have proposed the optimal power allocations and FSO fronthaul selection methods in cloud small-cell mm-Wave network. Moreover, wireless-over-fiber and FSO-over-fiber communication approaches have been studied in [27] and [28]. In addition, [29] has presented a hybrid data broadcasting system based on passive optical network (PON) and FSO backhauls. The performance of the wireless network based on FSO and fiber backhaul links has been investigated in [30] and [31], where the impacts of wireless co-channel interference, FSO pointing error, and optical fiber nonlinearity have been taken into account. Recently, the CF-mMIMO approach for *indoor* visible light communication has been studied in [32] and [33] without considering the effects of limited-capacity fronthaul/backhaul links.

To have a lower-complexity signal processing and skip channel decoding at the relay nodes, i.e. the APs and the ANs in our system, instead of utilizing the well-known decode-and-forward relaying scheme one can use the classical amplify-and-forward (AF) relaying scheme to reduce

the deployment costs. On the other hand, to convert the received signal of the relay to another domain, e.g. radio-over-FSO or FSO-over-*fiber* optics, a clipping model could be used for signal transformation [24], [34]–[37]. Thus, the relay nodes not only applies the AF scheme but also convert the received signals domain. Moreover, in practice, communication systems suffer from various non-idealities, such as phase noise, impedance mismatch, I/Q imbalance, quantization, and non-linearity of analog components [12]. Although by investing on high-quality devices or applying more complex signal processing at cost of increasing the deployment costs, still some non-negligible errors might remain. These errors are named hardware impairment (HI) [38]. Therefore, to propose a cost-efficient mMIMO network, analyzing the system's performance subject to the HI model has gained research interest [39]–[44]. Previous studies have also investigated impacts of the HI at transmitter, relay, and receiver sides [40]–[44].

To the best of our knowledge, performance of CF-mMIMO and UC-mMIMO networks with two layer of optical fronthaul and backhaul links subject to different hardware models have not been investigated in the literature. In this paper, we derive the uplink achievable rates of the CF- and UC-mMIMO wireless networks wherein FSO fronthaul links connect distributed APs to aggregation nodes (ANs), and optical fiber backhaul links connect ANs to a central processing unit (CPU). Moreover, clipping and HI models at APs and ANs are considered to convert RF signal to FSO and FSO ones to optical fiber signal forms. The main contributions of the paper are summarized as follows.

- Closed-form uplink achievable data rates are derived by employing maximum-ratio-combining (MRC) and use-and-then-forget (UatF) techniques separately for the CF- and UC-mMIMO wireless networks. Also, the effects of impairments noises in conjunction with the impacts of weather-dependent FSO channels are considered in our analysis.
- Optimal power allocations at users, and gain coefficients assignments at APs and ANs are investigated to maximize the uplink sum-rates of the two proposed networks subject to the maximum per-user transmit power and the maximum optical transmission powers at APs and ANs. To overcome the non-convexity of the optimization problem, we suggest a heuristic solution based on the geometric programming (GP) technique.
- Spectral- and energy-efficiency of the two types of networks, i.e. CF- and UC-mMIMO, are compared with clipping and HI models from various perspectives. Also, the performance of the networks are compared for various number APs, ANs, served users, and various weather conditions which affects FSO links.

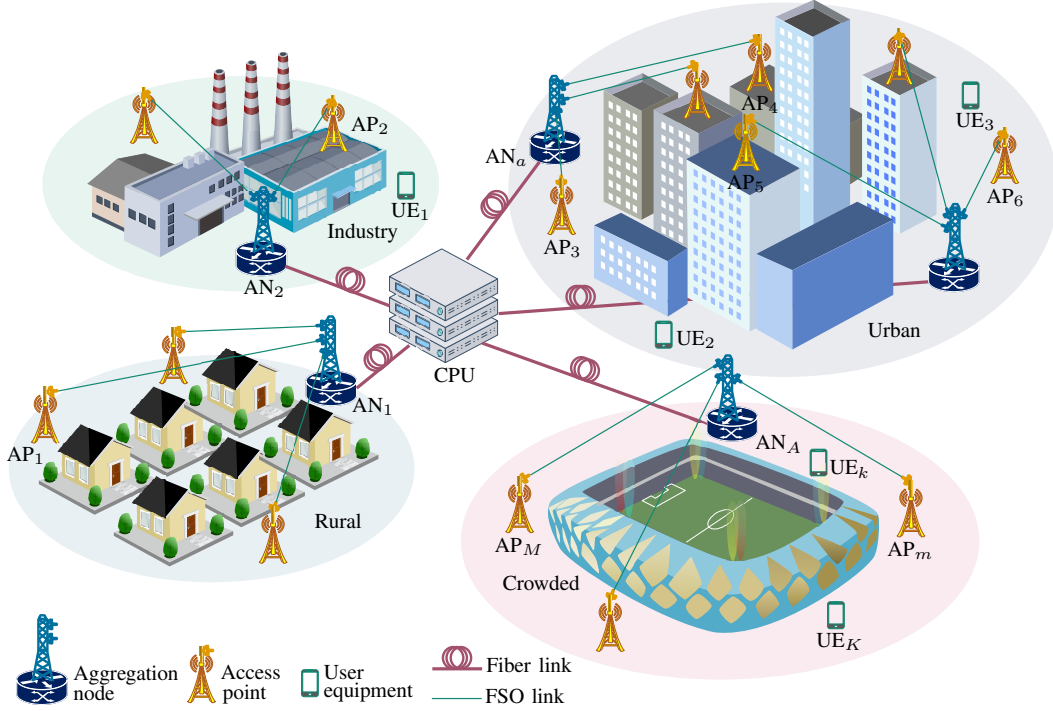


Fig. 1. CF-mMIMO wireless network with FSO fronthaul and fiber backhaul links.

*Organization:* Section II introduces the CF- and UC-mMIMO networks with FSO fronthaul links and optical fiber backhaul links under clipping and HI models. Channel training and data transmission are represented in Section III. Uplink achievable data rates are derived in Section IV. Section V presents the power allocations and gain coefficients assignments, and Section VI represents numerical results and discussions. Finally, the paper is concluded in Section VII.

*Notation:*  $\mathbf{x} \in \mathbb{C}^{n \times 1}$  denotes a vector in an  $n$ -dimensional complex space,  $\mathbb{E}\{\cdot\}$  is the expectation operator, and  $[\cdot]^T$  stands for the transpose. Also,  $y \sim \mathcal{N}(m, \sigma^2)$  and  $z \sim \mathcal{CN}(m, \sigma^2)$  respectively denote real-valued and complex symmetric Gaussian random variables (RVs) with mean  $m$  and variance  $\sigma^2$ .

## II. SYSTEM MODEL

We consider a distributed mMIMO network wherein  $M$  single-antenna APs simultaneously serve  $K$  single-antenna UEs at the same time–frequency resources, wherein the users are located over a wide area of different regions, e.g. urban and rural areas, industrial estates, and crowded places, c.f. Fig. 1. Thus to cover the whole region, it is also assumed that there are  $A$  aggregation nodes (ANs) to gather data form clusters of APs through FSO links, named as *fronthaul* links,

and then each AN transmits the received signal to the CPU via an optical fiber link, which is called *backhaul*. To analyze the performance of uplink data transmission for the proposed network, we consider two approaches; (a) a cell-free setup and (b) a user-centric one. Moreover, to acquire channel state information (CSI), each of the coherence intervals, i.e. coherence time and coherence bandwidth, is divided into two phases; uplink channel training to estimate the access channels between each of the UE–AP pair, and uplink data transmission. Without loss of generality, it is also assumed that the CPU has full-CSI of fronthaul and backhaul links at each time interval due to the fixed-distance fronthaul links and stable weather conditions.

Before investigating achievable rates analysis, we provide channel modelings and hardware models in the following subsections.

#### A. Access Channel

Wireless access channel between the  $k$ th UE and the  $m$ th AP is conventionally modeled by [4]

$$g_{mk} = \beta_{mk}^{1/2} h_{mk}, \text{ for } m = 1, 2, \dots, M \text{ and } k = 1, 2, \dots, K, \quad (1)$$

where  $\beta_{mk}$  and  $h_{mk}$  respectively represent large- and small-scale fading coefficients, where  $h_{mk} \sim \mathcal{CN}(0, 1)$  are independent and identically distributed (i.i.d) random variables.

#### B. Fronthaul Channel

Since each AP is connected to only one aggregation node via a FSO link, we define  $\mathcal{M}(a)$  to denote the set of served APs by  $a$ th AN for  $a = 1, 2, \dots, A$ , such that  $\sum_{a=1}^A \mathcal{M}(a) = M$ . To model the FSO channel between  $a$ th AN and the served  $m$ th AP for  $m \in \mathcal{M}(a)$ , we have

$$h_{am} = e^{-\gamma d_{am}} h_{t,am}, \quad (2)$$

where  $d_{am}$  represents the distance between  $a$ th AN and the  $m$ th AP, and  $\gamma$  [dB/km] denotes attenuation coefficient depending on the weather conditions. Furthermore,  $h_{t,am}$  models the atmospheric turbulence<sup>1</sup>. Since the APs are distributed in a given area, and each AN is located to serve its neighboring APs, it is assumed that  $d_{am} \leq 1$  [km]. Thus, under weak turbulence

<sup>1</sup>Here, it is assumed to employ the automatic beam tracking mechanism at the receiver. Since the short-range of fronthaul links, the bore sight pointing error, which is mainly due to building sway, beam wandering in the atmosphere, and misalignment receiver beam tracking [15], becomes negligible, i.e.  $h_{p,am} \simeq 1$  [24].

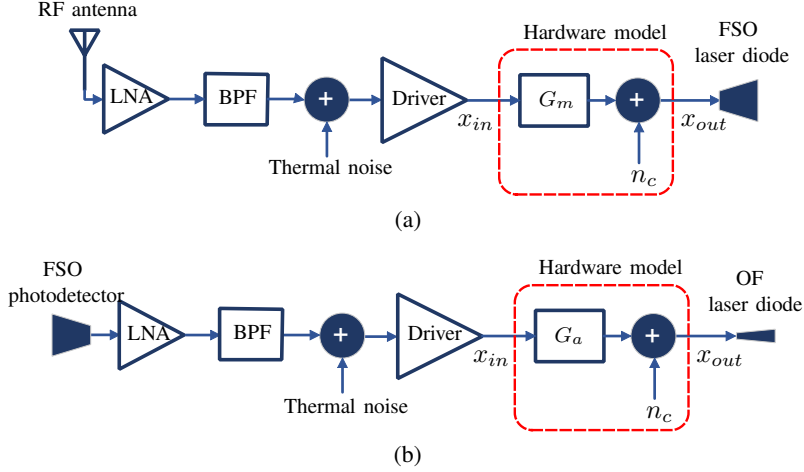


Fig. 2. The simplified signal transition diagram under hardware models at (a)  $m$ th AP and (b)  $a$ th AN.

condition, the log-normal distribution is applied with probability distribution function (p.d.f) of [24], [45]

$$f_{h_t,am}(h_t) = \frac{1}{2h_t\sqrt{2\pi\delta_{l,am}^2}} \exp\left(-\frac{(\ln(h_t) + 2\delta_{l,am}^2)^2}{8\delta_{l,am}^2}\right), \quad (3)$$

wherein  $\delta_{l,am}^2 = 0.307C_n^2k^{7/6}d_{am}^{11/6}$  denotes the log-amplitude variance of the plane wave while  $C_n^2$  represents the index of refraction structure, and  $k = 2\pi/\lambda$ .

### C. Hardware Models

To convert RF signals to optical ones at each AP and also to adjust FSO signals to optical fiber forms at each AN, we apply a generic model in which the noisy distorted signal is given by

$$x_{out} = Gx_{in} + n_c, \quad (4)$$

where  $G \in \{G_m, G_a\}$  denotes gain coefficients at  $m$ th AP and  $a$ th AN, respectively. Furthermore,  $x_{in} \sim \mathcal{N}(0, \delta^2)$  is the input signal,  $x_{out}$  represents the output signal, and  $n_c \sim \mathcal{CN}(0, \delta_c^2)$  denotes the impairment noise. The signal transition diagram under hardware models is simply illustrated in Fig. 2. Here, we investigate two types of hardware models; clipping and HI models.

1) *Clipping Model*: The received RF signal at each AP is firstly clipped and then a DC bias is added to make it non-negative. Then, the amplified signal is transmitted with a high-performance laser diode over the FSO link. This technique is named radio over FSO (RoFSO). Similarly at each AN, the photodetector converts the received FSO signal to an electrical one,

and then the signal is transformed to a non-negative clipped version and emitted through the optical fiber link by employing the laser diode. This technique is called FSO over optical fiber (FSoF). Eventually, to formulate the clipping model, we have  $G = \mu_c \lambda$ , where  $\lambda$  depicts the laser's gain, and  $\mu_c$  represents the clipping coefficient such that [24]

$$\mu_c = \text{erf}\left(\frac{B_c}{\sqrt{2\lambda^2\delta^2}}\right), \quad (5)$$

where  $\text{erf}(\cdot)$  is the error function, and  $B_c$  represents the clipping level. Moreover, variance of the clipping noise is given by [24]

$$\delta_c^2 = B_c^2(2 - \mu_c) + \lambda^2\delta^2(1 - \mu_c)\mu_c - \sqrt{\frac{2B_c^2\lambda^2\delta^2}{\pi}} \exp\left(-\frac{B_c^2}{2\lambda^2\delta^2}\right). \quad (6)$$

2) *Hardware Impairment Model:* The non-linear operations of communication components can also be modeled by HI. We apply the HI model, as an alternative to the clipping model, to propose a general non-ideal signal conversation mechanism at each node as a function of quality and distortion parameters. To formulate the HI model, we set  $G = \xi^{1/2}$ , where  $\xi \in [0, 1]$  represents the hardware quality factor,  $\xi = 1$  means *ideal* hardware and  $\xi = 0$  indicates the *useless* one. In this model,  $n_c \sim \mathcal{CN}(0, (1 - \xi)\delta^2)$  denotes the distortion noise which is independent of the input signal, and we also have  $\mathbb{E}\{|x_{out}|^2\} = \mathbb{E}\{|x_{in}|^2\} = \delta^2$  [12], [46].

### III. CHANNEL TRAINING AND DATA TRANSMISSION

In the CF- and UC-mMIMO networks, each coherence interval is divided into two phases; uplink channel training and uplink data transmission. In the following section, we first represent the uplink channel training phase to attain the estimation of wireless channel coefficients. Then, the users' uplink data transmission is investigated.

#### A. Uplink Channel Training

To obtain the CSI, UEs transmit uplink channel training sequences. After some mathematical computations and compression, each AP's converted FSO signal vector is delivered to the served AN via its fronthaul link. Similarly, after the same procedure, the reformed optical signal vector is transmitted from that AN to the CPU via its optical fiber backhaul link. Finally, wireless channel estimations are performed at the CPU. It is assumed that channel coefficients are constant over each coherence interval. Fig. 3 illustrates simplified channel training flow over the studied network. Hereafter, we discuss the obtained pilot signals at nodes and connection links.

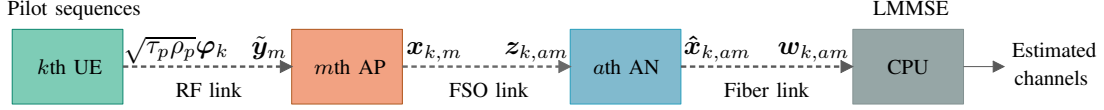


Fig. 3. Simplified channel training flow over the studied network.

1) *Pilot Signals from UEs to APs:* Let us denote  $T$  as the length of the coherence interval. Throughout the uplink training phase, all UEs transmit their  $\tau_p$ -length mutually orthogonal pilot sequences  $\sqrt{\tau_p \rho_p} \varphi_k \in \mathbb{C}^{\tau_p \times 1}$  for  $k = 1, 2, \dots, K$ , where  $\tau_p = K \leq T$ , and  $\|\varphi_k\|^2 = 1$ . Therefore, the  $\tau_p \times 1$  received pilot vector at  $m$ th AP is given by

$$\mathbf{y}_{p,m} = \sqrt{\tau_p \rho_p} \sum_{k=1}^K g_{mk} \varphi_k + \boldsymbol{\omega}_{p,m}, \quad (7)$$

where  $\rho_p$  represents the pilot transmission power, and  $\boldsymbol{\omega}_{p,m} \sim \mathcal{CN}(0, \sigma_{p,m}^2 \mathbf{I}_{\tau_p})$  denotes additive noise vector with independent and identically distributed (i.i.d.) elements. Afterward, the received signal at  $m$ th AP is multiplied with the conjugate-transpose of the  $k$ th pilot sequence for  $k$ th UE as

$$\tilde{y}_{p,mk} = \varphi_k^H \mathbf{y}_{p,m} = \sqrt{\tau_p \rho_p} \sum_{k'=1}^K g_{mk'} \varphi_k^H \varphi_{k'} + \omega'_{p,mk}, \quad (8)$$

where  $\omega'_{p,mk} = \varphi_k^H \boldsymbol{\omega}_{p,m}$ .

2) *Pilot Signals from APs to ANs:* To forward  $\tilde{y}_{p,mk}$  to the CPU to perform channel estimation, we firstly need to compress the vector of  $\tilde{\mathbf{y}}_{p,m} = [\tilde{y}_{p,m1}, \tilde{y}_{p,m2}, \dots, \tilde{y}_{p,mK}]^T \in \mathbb{C}^{K \times 1}$  at  $m$ th AP which is converted to the  $K \times 1$  FSO signal vector as

$$\mathbf{x}_{p,m} = G_m \tilde{\mathbf{y}}_{p,m} + \mathbf{n}_{p,m}^{\text{FSO}}, \quad (9)$$

where  $G_m$  depicts the gain coefficient at  $m$ th AP. Moreover,  $\mathbf{n}_{p,m}^{\text{FSO}} \sim \mathcal{CN}(0, \delta_{p,m}^2 \mathbf{I}_K)$  denotes the impairment noise vector. Thus, the  $K \times 1$  received vector at  $a$ th AN from  $m$ th AP for  $m \in \mathcal{M}(a)$  is given by

$$\mathbf{z}_{p,am} = R_{\text{FSO}} h_{am} \mathbf{x}_{p,m} + \mathbf{v}_{p,a}^{\text{FSO}}, \quad (10)$$

where  $R_{\text{FSO}}$  denotes the responsibility of the FSO photodetector, and  $\mathbf{v}_{p,a} \sim \mathcal{CN}(0, \psi_a^2 \mathbf{I}_K)$  models the additive noise vector at the FSO receiver.

3) *Pilot Signals from ANs to CPU:* To merely forward the received compressed pilot signals from the served  $m$ th AP to the CPU via OF-based backhaul link,  $a$ th AN transmits the following

signal

$$\hat{\mathbf{x}}_{p,am} = G_a \mathbf{z}_{p,am} + \mathbf{n}_{p,am}^{\text{OF}}, \quad (11)$$

where  $G_a$  and  $\lambda_a$  denotes the gain coefficient at  $a$ th AN, while  $\mathbf{n}_{p,am}^{\text{OF}} \sim \mathcal{CN}(0, \delta_{p,am}^2 \mathbf{I}_K)$  represents the impairment noise vector. Therefore, the received signal vector at the CPU becomes

$$\mathbf{w}_{p,am} = R_{\text{OF}} \hat{\mathbf{x}}_{p,am} + \mathbf{v}_p^{\text{OF}}, \quad (12)$$

where  $R_{\text{OF}}$  indicates the responsibility of the OF photodetector, and  $\mathbf{v}_p \sim \mathcal{CN}(0, \phi_{\text{CPU}}^2 \mathbf{I}_K)$  denotes the additive noise vector at the OF receiver. Finally, by use of (8)–(12), the received noisy version of pilot signal of the  $k$ th UE from  $a$ th AN and  $m$ th AP for  $m \in \mathcal{M}(a)$  at the CPU becomes

$$w_{p,amk} = \sqrt{\tau_p \rho_p} A_{am} h_{am} \sum_{k'=1}^K g_{mk'} \boldsymbol{\varphi}_k^H \boldsymbol{\varphi}_{k'} + n_{p,amk}^{\text{all}}, \quad (13)$$

where  $n_{p,amk}^{\text{all}} \sim \mathcal{CN}(0, \Omega_{p,amk}^2)$  represents the overall noise added to the desired pilot signal with

$$\begin{aligned} \Omega_{p,amk}^2 &= \mathbb{E} \left\{ \left| A_{am} h_{am} \omega'_{p,mk} + B_a h_{am} n_{p,mk}^{\text{FSO}} + C_a v_{p,ak}^{\text{FSO}} + R_{\text{OF}} n_{p,amk}^{\text{OF}} + v_{p,k}^{\text{OF}} \right|^2 \right\} \\ &= A_{am}^2 \Gamma_{am}^2 \sigma_{p,m}^2 + B_a^2 \Gamma_{am}^2 \delta_{p,m}^2 + C_a^2 \psi_a^2 + R_{\text{OF}}^2 \delta_{p,am}^2 + \phi_{\text{CPU}}^2, \end{aligned} \quad (14)$$

where

$$A_{am} = R_{\text{OF}} R_{\text{FSO}} G_m G_a, \quad B_a = R_{\text{OF}} R_{\text{FSO}} G_a, \quad C_a = R_{\text{OF}} G_a,$$

and for the  $n$ th moment of the log-normally distributed random variable  $h_{am}$ , we have

$$\Gamma_{am}^n := \mathbb{E} \{ |h_{am}|^n \} = \exp(2n(n-1)\delta_{l,am}^2 - n\gamma d_{am}). \quad (15)$$

One can show that all terms in the overall additive noise are mutually uncorrelated. So, the variance of the noise given in (14) becomes equal to the sum of the variances of the superimposed noises.

4) *Wireless Channel Estimation:* To obtain wireless channel coefficients at the CPU, the linear minimum mean square error (LMMSE) estimation is performed at the CPU. Thus, the estimated channel between  $k$ th UE and  $m$ th AP, which is served by  $a$ th AN, is derived as

$$\tilde{g}_{mk}^a = \frac{\mathbb{E} \{ w_{p,amk} g_{mk}^* \}}{\mathbb{E} \{ |w_{p,amk}|^2 \}} w_{p,amk} =: \zeta_{mk}^a w_{p,amk}, \quad (16)$$

where

$$\zeta_{mk}^a = \frac{\sqrt{\tau_p \rho_p} A_{am} \Gamma_{am} \beta_{mk}}{\tau_p \rho_p A_{am}^2 \Gamma_{am}^2 \sum_{k'=1}^K \beta_{mk'} + \Omega_{p,amk}^2}. \quad (17)$$

Due to the product of log-normal and Gaussian random variables in  $w_{p,amk}$ , the LMMSE is a sub-optimal channel estimation technique, and the variance of  $\tilde{g}_{mk}^a$  is

$$\gamma_{mk}^a := \mathbb{E} \{ |\tilde{g}_{mk}^a|^2 \} = \sqrt{\tau_p \rho_p} A_{am} \Gamma_{am} \beta_{mk} \zeta_{mk}^a. \quad (18)$$

### B. Uplink Data Transmission

For the uplink data transmission, received signals at APs are converted to FSO ones and transmitted to the served ANs through fronthaul links. Later, each AN transforms the received signals to optical signals and transmits to the CPU via its backhaul link. Finally, data recovery of users are performed at the CPU.

1) *Data Signals from UEs to APs:* In the uplink data transmission phase, all  $K$  UEs simultaneously transmit their data on the same time-frequency resource element. Let  $s_k \sim \mathcal{CN}(0, 1)$  denotes the transmission symbol of  $k$ th UE weighted by power control coefficient  $\eta_k \in [0, 1]$ . Therefore, the received signal at  $m$ th AP is given by

$$y_{u,m} = \sqrt{\rho_u} \sum_{k=1}^K \sqrt{\eta_k} g_{mk} s_k + \omega_{u,m}, \quad (19)$$

where  $\rho_u$  represents the maximum signal transmission power, and  $\omega_{u,m} \sim \mathcal{CN}(0, \sigma_{u,m}^2)$  indicates the additive noise.

2) *Data Signals from APs to ANs:* The compressed signal at  $m$ th AP is optically forwarded to the connected AN by applying the hardware models as

$$x_{u,m} = G_m y_{u,m} + n_{u,m}^{\text{FSO}}, \quad (20)$$

where  $n_{u,m}^{\text{FSO}} \sim \mathcal{CN}(0, \delta_{u,m}^2)$  denotes the impairment noise. Therefore, the received optical signal at  $a$ th AN from  $m$ th AP for  $m \in \mathcal{M}(a)$  is given by

$$z_{u,am} = R_{\text{FSO}} h_{am} x_{u,m} + v_{u,a}^{\text{FSO}}, \quad (21)$$

where  $R_{\text{FSO}}$  and  $v_{u,a}^{\text{FSO}} \sim \mathcal{CN}(0, \psi_a^2)$  respectively denote the responsibility of FSO photodetector and the additive noise at the receiver.

3) *Data Signals from ANs to CPU*: Similar to (20), the transmitted optical signal at  $a$ th AN is given by

$$\hat{x}_{u,am} = G_a z_{u,am} + n_{u,am}^{\text{OF}}, \quad (22)$$

where  $n_{u,am}^{\text{OF}} \sim \mathcal{CN}(0, \delta_{u,am}^2)$  is the impairment noise. Thus, the received uplink data signal at the CPU becomes

$$w_{u,am} = R_{\text{OF}} \hat{x}_{u,am} + v_u^{\text{OF}}, \quad (23)$$

where  $R_{\text{OF}}$  represents the OF photodetector's responsibility coefficient, and  $v_u^{\text{OF}} \sim \mathcal{CN}(0, \phi_{\text{CPU}}^2)$  denotes the additive noise at the OF receiver. Finally, by using (19)–(23), the received data signal of  $k$ th UE from  $a$ th AN and  $m$ th AP for  $m \in \mathcal{M}(a)$  at the CPU is rewritten as

$$w_{u,am} = \sqrt{\rho_u} A_{am} h_{am} \sum_{k=1}^K \sqrt{\eta_k} g_{mk} s_k + n_{u,am}^{\text{all}}, \quad (24)$$

where  $n_{u,am}^{\text{all}} \sim \mathcal{CN}(0, \Omega_{u,am}^2)$  is the overall noise added to the received data, where

$$\begin{aligned} \Omega_{u,am}^2 &= \mathbb{E} \left\{ \left| A_{am} h_{am} \omega_{u,m} + B_a h_{am} n_{u,m}^{\text{FSO}} + C_a v_{u,a}^{\text{FSO}} + R_{\text{OF}} n_{u,am}^{\text{OF}} + v_u^{\text{OF}} \right|^2 \right\} \\ &= A_{am}^2 \Gamma_{am}^2 \sigma_{u,m}^2 + B_a^2 \Gamma_{am}^2 \delta_{u,m}^2 + C_a^2 \psi_a^2 + R_{\text{OF}}^2 \delta_{u,am}^2 + \phi_{\text{CPU}}^2. \end{aligned} \quad (25)$$

As provided in (14), all terms of the overall additive noise are mutually uncorrelated. Thus, the variance of the noise given in (25) becomes equal to the sum of the variances of superimposed noises.

#### IV. ACHIEVABLE RATES ANALYSIS

In the following section, we present the user data detection and uplink achievable data rates for two scenarios of UC-mMIMO and CF-mMIMO networks.

##### A. Data Recovery

Here, we propose a data detection method based on the estimated wireless channel coefficients derived in (16). After the CPU receives the uplink data signal given in (24) from all ANs, it applies the MRC technique to recover the data symbols of all users. In the following, we investigate the two scenarios.

1) *UC-mMIMO Network*: For the UC-mMIMO network, the CPU exerts a measuring mechanism based on the estimated wireless channels to specify a cluster of UEs connected to each AP. So, we let  $\mathcal{K}(m)$  denotes the set of served UEs by  $m$ th AP, and  $\mathcal{M}(k)$  is the set of APs communicated with  $k$ th UE, which is defined as [8]

$$\mathcal{M}(k) = \{m : k \in \mathcal{K}(m)\}. \quad (26)$$

By employing the estimated channels, there are various measuring mechanisms to sort the served UEs in UC-mMIMO approach. However, we apply a mechanism by which the CPU classifies the estimated channel gains for every AP in descending order and chooses a specific number of the served UEs named  $N_{UC}$ . Therefore, to recover the data symbol of  $k$ th UE  $s_k$ , we have

$$r_{u,k} = \sum_{a=1}^A \sum_{m \in \mathcal{M}_k(a)} w_{u,am} \tilde{g}_{mk}^{a*} \quad (27a)$$

$$= \sqrt{\rho_u} \sum_{a=1}^A \sum_{m \in \mathcal{M}_k(a)} A_{am} h_{am} \sum_{k'=1}^K \sqrt{\eta_{k'}} g_{mk'} \tilde{g}_{mk}^{a*} s_{k'} + \sum_{a=1}^A \sum_{m \in \mathcal{M}_k(a)} n_{u,am}^{all} \tilde{g}_{mk}^{a*} \quad (27b)$$

$$= \sqrt{\rho_u \eta_k} \sum_{a=1}^A \sum_{m \in \mathcal{M}_k(a)} A_{am} h_{am} g_{mk} \tilde{g}_{mk}^{a*} s_k + \sqrt{\rho_u} \sum_{a=1}^A \sum_{m \in \mathcal{M}_k(a)} A_{am} h_{am} \sum_{\substack{k'=1 \\ k' \neq k}}^K \sqrt{\eta_{k'}} g_{mk'} \tilde{g}_{mk}^{a*} s_{k'} + \sum_{a=1}^A \sum_{m \in \mathcal{M}_k(a)} n_{u,am}^{all} \tilde{g}_{mk}^{a*}, \quad (27c)$$

where  $\mathcal{M}_k(a) = \mathcal{M}(a) \cap \mathcal{M}(k)$ .

2) *CF-mMIMO Network*: In the CF-mMIMO network, we employ the same data detection method as in (27). However, in this approach, since each AP serves all UEs, we just need to use  $\mathcal{M}_k(a) = \mathcal{M}(a)$  in the expressions.

### B. Uplink Achievable Data Rates

Through this subsection, we derive uplink achievable data rates for UC-mMIMO and CF-mMIMO networks under clipping and HI models. To relax the availability of the full instantaneous CSI at a user, we exploit the well-known use-and-then-forget (UatF) technique [2]. Nevertheless, it is sufficient to know only the effective channel's statistical average.

1) *UC-mMIMO Network*: For the UC-mMIMO network, we rewrite (27) as follows

$$r_{u,k} = \text{DS}_k s_k + \underbrace{\text{BU}_k s_k + \sum_{\substack{k'=1 \\ k' \neq k}}^K \text{IUI}_{kk'} s_{k'}}_{\text{effective noise}} + \text{N}_k, \quad (28)$$

where

- $\text{DS}_k$  denotes the desired signal of  $k$ th user

$$\text{DS}_k = \sqrt{\rho_u \eta_k} \mathbb{E} \left\{ \sum_{a=1}^A \sum_{m \in \mathcal{M}_k(a)} A_{am} h_{am} g_{mk} \tilde{g}_{mk}^{a*} \right\}, \quad (29)$$

- $\text{BU}_k$  is the beamforming uncertainty of  $k$ th UE due to the statistical knowledge of CSI

$$\text{BU}_k = \sqrt{\rho_u \eta_k} \left( \sum_{a=1}^A \sum_{m \in \mathcal{M}_k(a)} A_{am} h_{am} g_{mk} \tilde{g}_{mk}^{a*} - \mathbb{E} \left\{ \sum_{a=1}^A \sum_{m \in \mathcal{M}_k(a)} A_{am} h_{am} g_{mk} \tilde{g}_{mk}^{a*} \right\} \right), \quad (30)$$

- $\text{IUI}_{kk'}$  represents the inter-user interference from  $k'$  UE

$$\text{IUI}_{kk'} = \sqrt{\rho_u \eta_{k'}} \sum_{a=1}^A \sum_{m \in \mathcal{M}_k(a)} A_{am} h_{am} g_{mk'} \tilde{g}_{mk'}^{a*}, \quad (31)$$

- $\text{N}_k$  indicates the composition of effective noise

$$\text{N}_k = \sum_{a=1}^A \sum_{m \in \mathcal{M}_k(a)} n_{u,am}^{all} \tilde{g}_{mk}^{a*}. \quad (32)$$

One can show that all elements given in (28) are mutually uncorrelated. From the information theoretic perspective, to analyze the worst-case scenario, we assume that the effective noise is modeled by an equivalent Gaussian random variable. Thus, the uplink achievable data rates of  $k$ th UE is given by

$$R_{u,k} = \log_2 (1 + \text{SINR}_k) \text{ [bps/Hz]}, \quad (33)$$

where

$$\text{SINR}_k = \frac{|\text{DS}_k|^2}{\mathbb{E}\{|\text{BU}_k|^2\} + \sum_{\substack{k'=1 \\ k' \neq k}}^K \mathbb{E}\{|\text{IUI}_{kk'}|^2\} + \mathbb{E}\{|\text{N}_k|^2\}}. \quad (34)$$

In the following Theorem, the SINR of the  $k$ th user is computed.

$$\text{SINR}_k = \frac{\eta_k \left( \sum_{a=1}^A \sum_{m \in \mathcal{M}_k(a)} G_a G_m A_{amk} \right)^2}{\sum_{a=1}^A \sum_{m \in \mathcal{M}_k(a)} G_a^2 G_m^2 \left( \eta_k B_{amk} + \sum_{\substack{k'=1 \\ k' \neq k}}^K \eta_{k'} C_{amkk'} \right) + D_k}, \quad (35)$$

$$\Lambda_{amk} = \Gamma_{am}^2 \beta_{mk} + (\Gamma_{am}^2 - (\Gamma_{am})^2) \gamma_{mk}^a, \quad \Lambda'_{amk} = \frac{\Gamma_{am}^4}{(\Gamma_{am})^2} \frac{(\gamma_{mk}^a)^2}{\beta_{mk}} + \Gamma_{am}^2 (\zeta_{mk}^a)^2 \Omega_{p,amk}^2,$$

$$D_k = \sum_{a=1}^A \sum_{m \in \mathcal{M}_k(a)} \gamma_{mk}^a \Omega_{u,am}^2, \quad A_{amk} = \sqrt{\rho_u} R_{\text{OF}} R_{\text{FSO}} \Gamma_{am} \gamma_{mk}^a, \quad B_{amk} = \rho_u R_{\text{OF}}^2 R_{\text{FSO}}^2 \gamma_{mk}^a \Lambda_{amk},$$

$$\text{and } C_{amkk'} = \rho_u R_{\text{OF}}^2 R_{\text{FSO}}^2 \beta_{mk'} \Lambda'_{amk}.$$

**Theorem 1.** *The SINR of the  $k$ th UE is given by (35), shown at the top of this page.*

*Proof.* The proof is given in Appendix A.

2) *CF-mMIMO Network:* To compute the uplink data rates of the CF-mMIMO network, we just replace  $\mathcal{M}_k(a) = \mathcal{M}(a)$  in (35).

## V. RESOURCE ALLOCATION

In this section, we aim to maximize the network performance by efficiently allocating the power of each user and controlling the gain coefficients of access points and aggregation nodes under the clipping and hardware impairment models for the CF- and UC-mMIMO networks. Thereafter, the optimization problem is written as follows

$$\begin{aligned} \mathcal{P}_1 : \quad & \underset{\substack{\{\eta_k \geq 0\}_k, \\ \{G_m \geq 0\}_m, \{G_a \geq 0\}_a}}{\text{maximize}} \quad \frac{\tau - \tau_p}{\tau} \sum_{k=1}^K \log_2 (1 + \text{SINR}_k) \\ & \text{subject to} \quad \begin{cases} \mathcal{C}_1 : \eta_k \leq 1, \forall k, \\ \mathcal{C}_2 : \mathbb{E}\{|x_{u,m}|^2\} \leq P_{\text{max}}^{\text{FSO}}, \forall m, \\ \mathcal{C}_3 : \mathbb{E}\{|\hat{x}_{u,am}|^2\} \leq P_{\text{max}}^{\text{OF}}, \forall a, m \in \mathcal{M}(a), \end{cases} \end{aligned} \quad (36)$$

where  $P_{\text{max}}^{\text{FSO}}$  denotes the maximum FSO transmission power at each AP to satisfy the eye-safety regulations, and  $P_{\text{max}}^{\text{OF}}$  represents the maximum optical power in a single-mode fiber at each AN.

**Lemma 1.** *To convert the constraint  $\mathcal{C}_2$ , given in  $\mathcal{P}_1$ , to a monomial-formed expression, it is replaced by*

$$G_m^2 \left( \rho_u \sum_{k=1}^K \eta_k \beta_{mk} + \sigma_{u,m}^2 \right) \leq P_{\max}^{\text{FSO}}. \quad (37)$$

*Proof.* To derive the FSO transmission power, we have

$$\begin{aligned} \mathbb{E}\{|x_{u,m}|^2\} &= \mathbb{E}\left\{ \left| G_m \sqrt{\rho_u} \sum_{k=1}^K \sqrt{\eta_k} g_{mk} s_k + G_m \omega_{u,m} + n_{u,m} \right|^2 \right\} \\ &= G_m^2 \left( \rho_u \sum_{k=1}^K \eta_k \beta_{mk} + \sigma_{u,m}^2 \right) + \mathbb{E}\{|n_{u,m}|^2\} \leq P_{\max}^{\text{FSO}}. \end{aligned}$$

Therefore, we have

$$G_m^2 \left( \rho_u \sum_{k=1}^K \eta_k \beta_{mk} + \sigma_{u,m}^2 \right) \leq P_{\max}^{\text{FSO}} - \mathbb{E}\{|n_{u,m}|^2\} \leq P_{\max}^{\text{FSO}}.$$

Without of loss of generality, by replacing  $P_{\max}^{\text{FSO}} - \mathbb{E}\{|n_{u,m}|^2\}$  with  $P_{\max}^{\text{FSO}}$ , the feasible set becomes larger or equivalently we can assume higher maximum power. It is also worth noting that, numerical result indicates that the value of  $\mathbb{E}\{|n_{u,m}|^2\} \geq 0$  is also negligible compared to  $P_{\max}^{\text{FSO}}$ .

**Lemma 2.** *The constraint  $\mathcal{C}_3$  in  $\mathcal{P}_1$  is simplified as*

$$R_{\text{FSO}}^2 \Gamma_{am}^2 G_a^2 G_m^2 \left( \rho_u \sum_{k=1}^K \eta_k \beta_{mk} + \sigma_{u,m}^2 \right) + G_a^2 \psi_a^2 \leq P_{\max}^{\text{OF}}. \quad (38)$$

*Proof.* We use the same approach as Lemma 1.

Since the optimization problem  $\mathcal{P}_1$  is a non-convex and NP-hard problem, we employ the high-SINR approximation solving method [12]. By applying the approximation, the objective function is lower-bounded with  $\frac{\tau - \tau_p}{\tau} \log_2 \left( \prod_{k=1}^K \text{SINR}_k \right)$ . Moreover, because  $\frac{\tau - \tau_p}{\tau}$  is constant and

$$\begin{aligned}
\mathcal{P}_3 : \quad & \underset{\substack{\{w_k \geq 0\}_k, \{\eta_k \geq 0\}_k, \\ \{G_m \geq 0\}_m, \{G_a \geq 0\}_a}}{\text{maximize}} \quad \prod_{k=1}^K w_k \\
\text{subject to: } & \mathcal{C}_1 : \eta_k \leq 1, \forall k, \quad \mathcal{C}_2 : \frac{G_m^2 \left( \rho_u \sum_{k=1}^K \eta_k \beta_{mk} + \sigma_{u,m}^2 \right)}{P_{\max}^{\text{FSO}}} \leq 1, \forall m, \\
& \mathcal{C}_3 : \frac{R_{\text{FSO}}^2 \Gamma_{am}^2 G_a^2 G_m^2 \left( \rho_u \sum_{k=1}^K \eta_k \beta_{mk} + \sigma_{u,m}^2 \right)}{P_{\max}^{\text{OF}}} + \frac{G_a^2 \psi_a^2}{P_{\max}^{\text{OF}}} \leq 1, \forall a, m \in \mathcal{M}(a), \\
& \mathcal{C}_4 : w_k \frac{\sum_{a=1}^A \sum_{m \in \mathcal{M}_k(a)} G_a^2 G_m^2 B_{amk}}{\left( \sum_{a=1}^A \sum_{m \in \mathcal{M}_k(a)} G_a G_m A_{amk} \right)^2} + \frac{w_k \sum_{k' \neq k} \sum_{a=1}^A \sum_{m \in \mathcal{M}_k(a)} G_a^2 G_m^2 C_{amkk'}}{\eta_k \left( \sum_{a=1}^A \sum_{m \in \mathcal{M}_k(a)} G_a G_m A_{amk} \right)^2} \\
& \quad + \frac{w_k D_k}{\eta_k \left( \sum_{a=1}^A \sum_{m \in \mathcal{M}_k(a)} G_a G_m A_{amk} \right)^2} \leq 1, \forall k.
\end{aligned} \tag{40}$$


---

$\log_2(x) \leq x, \forall x$ , the optimization problem is reformulated as

$$\begin{aligned}
\mathcal{P}_2 : \quad & \underset{\substack{\{w_k \geq 0\}_k, \{\eta_k \geq 0\}_k, \\ \{G_m \geq 0\}_m, \{G_a \geq 0\}_a}}{\text{maximize}} \quad \prod_{k=1}^K w_k \\
\text{subject to } & \begin{cases} \mathcal{C}_1 : \eta_k \leq 1, \forall k, \\ \mathcal{C}_2 : G_m^2 \left( \rho_u \sum_{k=1}^K \eta_k \beta_{mk} + \sigma_{u,m}^2 \right) \leq P_{\max}^{\text{FSO}}, \forall m, \\ \mathcal{C}_3 : R_{\text{FSO}}^2 \Gamma_{am}^2 G_a^2 G_m^2 \left( \rho_u \sum_{k=1}^K \eta_k \beta_{mk} + \sigma_{u,m}^2 \right) + G_a^2 \psi_a^2 \leq P_{\max}^{\text{OF}}, \forall a, m \in \mathcal{M}(a), \\ \mathcal{C}_4 : w_k \leq \text{SINR}_k, \forall k. \end{cases}
\end{aligned} \tag{39}$$

By replacing (37)–(38) into  $\mathcal{P}_2$  and further mathematical manipulations, the optimization problem is rewritten as (40) at the top of this page. The optimization problem  $\mathcal{P}_3$  is a geometric program (GP) because the objective function has the form of a monomial (hence, also posynomial), and all the inequality constraints are posynomial functions and are less than or equal one. Thus,  $\mathcal{P}_3$  can be solved by using the available tools such as MOSEK in CVX.

TABLE I  
PROPOSED NETWORK SCENARIOS FOR NUMERICAL RESULTS.

Scenario	Network model	Hardware model
CFCL	CF-mMIMO	Clipping
CFHI	CF-mMIMO	Hardware impairment
UCCL	UC-mMIMO	Clipping
UCHI	UC-mMIMO	Hardware impairment

## VI. NUMERICAL RESULTS AND DISCUSSIONS

In the following section, we present numerical results to highlight the performance of CF- and UC-mMIMO networks based on clipping and HI models from energy- and energy-efficiency perspectives. Herein, the numerical results are presented and discussed based on four scenarios defined as Table I; CFCL, CFHI, UCCL, and UCHI. Conventionally, it is assumed that  $K=10$  UEs and  $M=100$  APs are uniformly distributed within an area of  $D=1 \times 1$  [km<sup>2</sup>], where  $A=4$  ANs are spread over a circle with radius (backhaul length) of 200 [m] and the constant angle of  $\pi/2$  [rad] between adjacent ANs. For the large-scale fading, we employ [12]

$$\beta_{mk} = \text{PL}_{mk} + \sigma_{sh} z_{mk}, \quad (41)$$

where  $\text{PL}_{mk}$  [dB] denotes the path-loss and  $\sigma_{sh} z_{mk}$  is the shadowing with standard deviation  $\sigma_{sh}$  [dB] and the shadowing correlation factor  $z_{mk}$ . By employing the conventional three-slope propagation model, we have [4], [12]

$$\text{PL}_{mk} = \begin{cases} -L - 35\log_{10}(d_{mk}), & d_{mk} > d_1 \\ -L - 15\log_{10}(d_1) - 20\log_{10}(d_{mk}), & d_0 < d_{mk} \leq d_1 \\ -L - 15\log_{10}(d_1) - 20\log_{10}(d_0), & d_{mk} \leq d_0 \end{cases} \quad (42)$$

where  $d_0$  and  $d_1$  are distance references,  $d_{mk}$  denotes the distance between  $m$ th AP and  $k$ th UE, and  $L$  [dB] is defined as follows

$$L = 46.3 + 33.9\log_{10}(f) - 13.82\log_{10}(h_{\text{AP}}) \\ - (1.1\log_{10}(f) - 0.7)h_{\text{UE}} + (1.56\log_{10}(f) - 0.8), \quad (43)$$

TABLE II  
NETWORK PARAMETERS FOR NUMERICAL RESULTS.

Parameter	Symbol	Value
Access radio frequency	$f$	1.9 [GHz]
System bandwidth	$B_s$	20 [MHz]
Antenna height of AP	$h_{AP}$	15 [m]
Antenna height of UE	$h_{UE}$	1.65 [m]
Path-loss model {minimum, maximum} distance references	$d_0$	{10, 50} [m]
Shadowing standard deviation	$\sigma_{sh}$	8 [dB]
Shadowing correlation coefficient	$\theta$	0.5
Decorrelation distance	$d_{dec}$	0.1 [km]
{Clear, rainy, snowy, foggy} weather attenuation coefficients	$\gamma_{Clear}$	{0.44, 0.523, 4.53, 50} [dB/km]
Fronthaul FSO wavelength	$\lambda$	1550 [nm]
Index of refraction structure	$C_n^2$	$5 \times 10^{-14}$ [ $m^{3/2}$ ]
UE's maximum pilot transmission power	$\rho_p$	100 [mWatt]
UE's maximum uplink data transmission power	$\rho_u$	100 [mWatt]
Length of time coherent interval	$T$	100
Clipping level	$B_c$	1
Responsibility of FSO receiver	$R_{FSO}$	0.5
Responsibility of OF receiver	$R_{OF}$	1
Maximum FSO transmission power	$P_{max}^{FSO}$	14 [dBm]
Maximum SMF optical power	$P_{max}^{OF}$	14 [dBm]
Number of served UEs by each AP	$N_{UC}$	10
Circuit power at $m$ th AP	$P_m$	0.2 [Watt]
Circuit power at $a$ th AN	$P_a$	0.5 [Watt]
Fronthaul's constant power of $m$ th AP	$P_{c,m}$	1 [Watt]
Backhaul's constant power of $a$ th AN	$P_{c,a}$	0.825 [Watt]
FSO fronthaul's traffic-dependent power of $m$ th AP	$P_{th,m}$	0.3 [Watt/Gbps]
OF backhaul's traffic-dependent power of $a$ th AN	$P_{bh,a}$	0.25 [Watt/Gbps]
Variance of AWGN noise at $a$ th AN	$\psi_a^2$	$10^{-14}$ [ $A^2$ ]
Variance of AWGN noise at CPU	$\phi_{CPU}^2$	$10^{-14}$ [ $A^2$ ]
Additive noise power at $m$ th AP	$\sigma_{p,m}^2$ or $\sigma_{u,m}^2$	$k_B \cdot T_0 \cdot B_s \cdot (F - 1)$
Boltzmann constant	$k_B$	$1.381 \times 10^{-23}$ [dB]
Noise temperature	$T_0$	290 [Kelvin]
Noise figure	$F$	9 [dB]

where  $f$  [MHz] represents access radio frequency,  $h_{AP}$  [m] and  $h_{UE}$  [m] are antenna heights of AP and UE, respectively. Also, the correlated shadowing model introduced in [4] is given by

$$z_{mk} = a_m \sqrt{\theta} + b_k \sqrt{1 - \theta}, \quad (44)$$

where  $\theta \in [0, 1]$ ,  $a_m \sim \mathcal{N}(0, 1)$  and  $b_k \sim \mathcal{N}(0, 1)$  are independent random variables which respectively model contribution to the shadowing due to the obstacles near to APs and the ones near to UEs. In this case,  $\theta = 0$  indicates the shadowing caused by each UE becomes equal at all APs, and for  $\theta = 1$ , the shadowing caused by each AP becomes similar for all UEs<sup>2</sup>. The parameters used for the numerical results are summarized in Table II; otherwise, they are clearly mentioned in the paper.

Fig. 4(a) depicts cumulative distribution function (CDF) versus the network's sum spectral efficiency (sum-SE) for two types of resource allocations. In one case, we consider constant gain coefficients for  $G_m = G_{\text{FSO}}$  and  $G_a = G_{\text{OF}}$  for  $m = 1, 2, \dots, M$  and  $a = 1, 2, \dots, A$ , and all users transmit signals with maximum powers which is called the full-power. On the other hand, we apply the optimal transmit power allocations of the users, and gain coefficients assignments at the APs and the ANs. The figure emphasizes that optimal resource allocation improves the performances of all investigated network scenarios. For instance, the resource allocation provides a 60% increase in sum-SE for UCHI scenario. In this figure, UCHI outperforms all UCCL, CFHI, and CFCL scenarios. To represent the figure, we assume unit gain coefficients.

Fig. 4(b) and Fig. 4(c) respectively depict the networks' sum-SE versus the gain coefficients at the APs, i.e.  $G_{\text{FSO}}$ , and at the ANs, i.e.  $G_{\text{OF}}$ , for the various scenarios. Without loss of generality and to take advantage of simple resource allocations, we apply two fair full-power and half-power allocations to compare the networks' performances. It is shown that the UC-mMIMO network outperforms the CF-mMIMO one, and thanks to the HI model, we have a higher sum-SE compared to the case that we apply the clipping model. Although the higher values of  $G_{\text{FSO}}$  or  $G_{\text{OF}}$  increases power of the desired signal, it also increases the power of the effective noise. Thus, the sum-SE saturates by increasing the gain coefficients.

Fig. 4(d) represents the sum-SE of the network versus UE's transmission power for the proposed scenarios with two different typical gain coefficients. In this figure, despite the rise of received desired signal's power by increasing the UE's transmission power, both interference and noise increase, so the sum-SE reaches its maximum and remains constant. For example, the sum-SE for CFCL and CFHI scenarios saturates with the transmission power of around 1 [dBWatt]

<sup>2</sup>For the covariances of  $a_m$  and  $b_k$ , we have [4]

$$\mathbb{E}\{a_m a_{m'}\} = 2^{-\frac{d_{AP}(m, m')}{d_{dec}}}, \quad \mathbb{E}\{b_k b_{k'}\} = 2^{-\frac{d_{UE}(k, k')}{d_{dec}}},$$

where  $d_{dec}$  is the decorrelation distance of the environment,  $d_{AP}(m, m')$  is the distance between  $m$ th and  $m'$ th APs, and  $d_{UE}(k, k')$  denotes the distance between  $k$ th and  $k'$ th UEs.

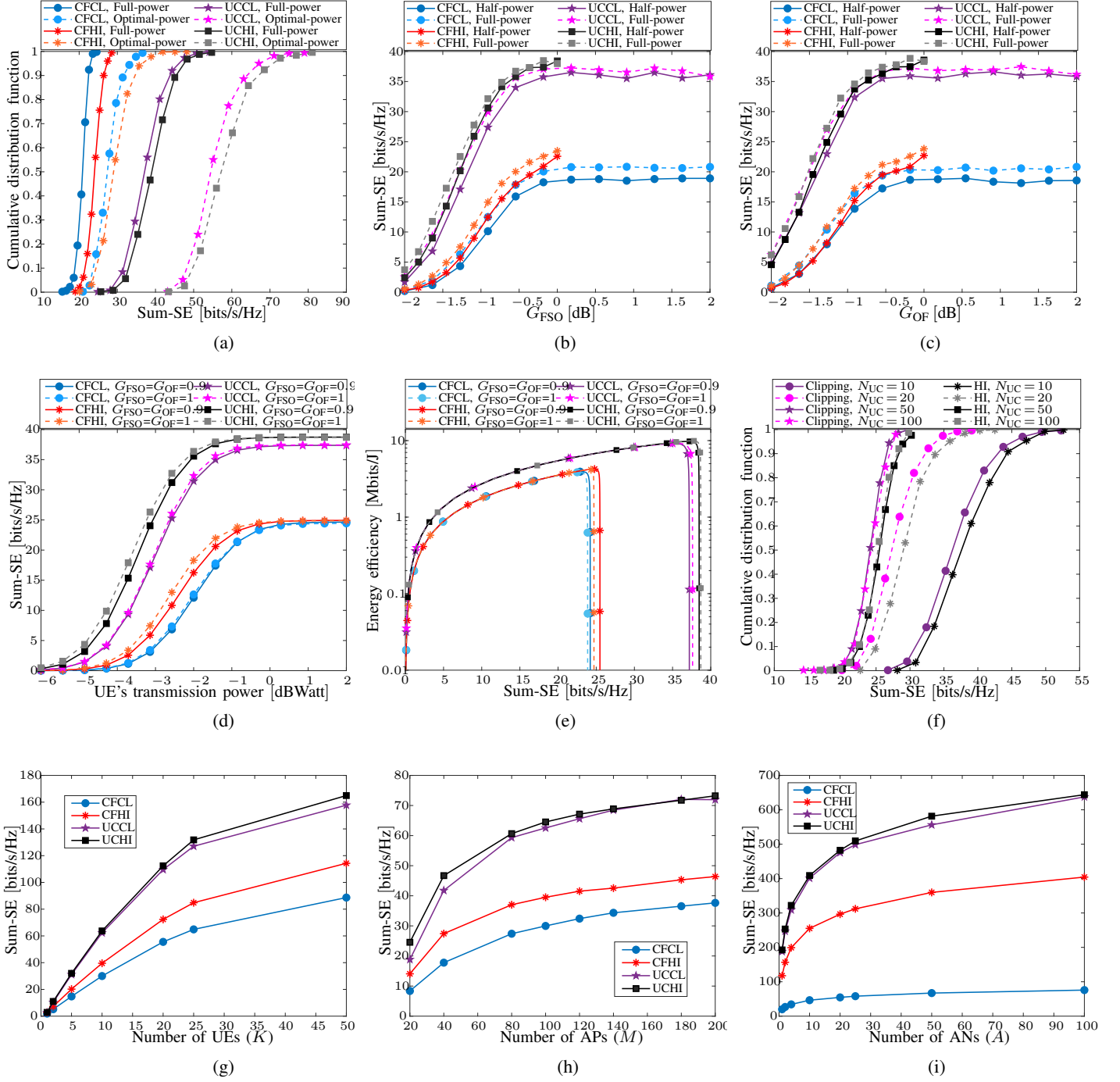


Fig. 4. (a): The CDF of the network's sum-SE with optimal power allocations and gain coefficients assignments, (b): The network's Sum-SE versus the AP's gain coefficient, (c): The network's Sum-SE versus the AN's gain coefficient, (d): The network's Sum-SE versus the user's transmission power, (e): The energy efficiency versus the sum-SE of the network, and (f): The CDF of the UC-mMIMO network's sum-SE for different number of served UEs by each AP, where we assume that  $K = 10$ ,  $M = 100$ , and  $A = 4$ . Moreover, (g): The sum-SE of the network versus the number of users for  $M = 100$  and  $A = 4$ , (h): The sum-SE of the network versus the number of access points for  $K = 10$  and  $A = 4$ , and (i): The sum-SE of the network versus the number of aggregation nodes for  $K = 10$  and  $M = 100$ .

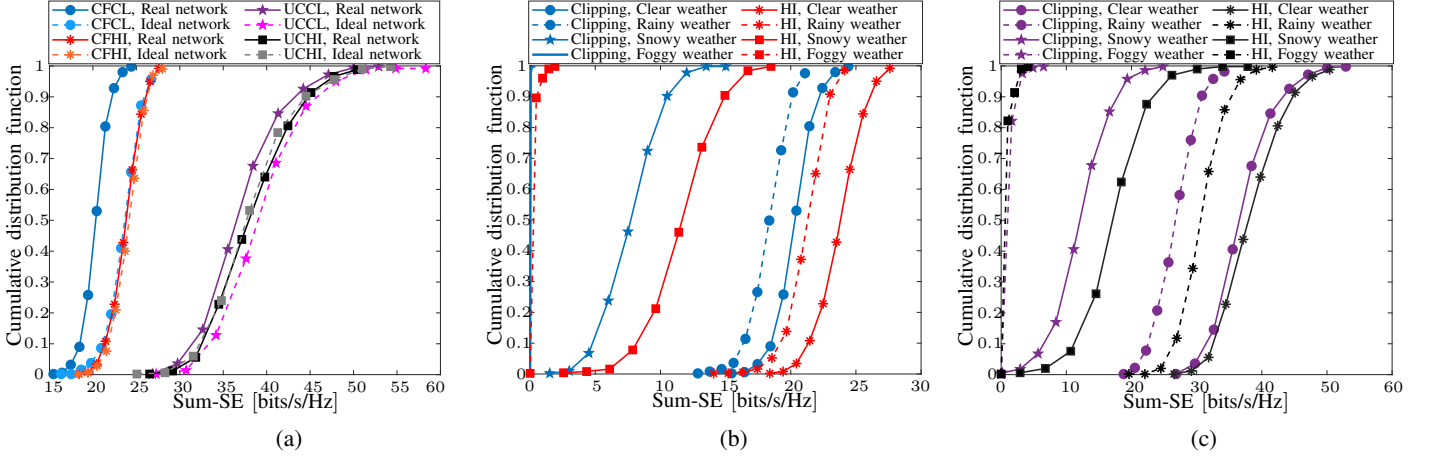


Fig. 5. (a): The CDF of the network's sum-SE and under real and ideal conditions. Also, the CDF of the network's sum-SE for different weather conditions of (b) CF-mMIMO and (c) UC-mMIMO networks. Herein, we assume that  $K = 10$ ,  $M = 100$ , and  $A = 4$ .

and 0 [dBWatt], respectively. Moreover, it is shown that the UC-mMIMO network has better performance than that of the CF-mMIMO one, and the HI model enhances the sum-SE for either specific values of UEs' transmission power compared to the clipping model.

Fig. 4(e) represents the energy efficiency (EE) versus the sum-SE of the network for various scenarios. The EE of the network is defined as [10]

$$EE = \frac{B_s \sum_{k=1}^K \log_2 (1 + \text{SINR}_k)}{P_{\text{net}}}, \quad (45)$$

with

$$\begin{aligned} P_{\text{net}} &= \underbrace{\rho_u \sum_{k=1}^K \eta_k}_{\text{users}} + \underbrace{\sum_{m=1}^M P_m + \sum_{m=1}^M (P_{c,m} + B_s R_{u,m} P_{\text{fh},m})}_{\text{access points and fronthaul links}} \\ &= \underbrace{\sum_{a=1}^A P_a + \sum_{a=1}^A (P_{c,a} + B_s R_{u,a} P_{\text{bh},a})}_{\text{aggregation nodes and backhaul links}}, \end{aligned} \quad (46)$$

where  $P_m$  and  $P_a$  signify the power consumed by circuit components of transceivers at  $m$ th AP and  $a$ th AN, respectively. Also,  $P_{c,m}$  and  $P_{\text{fh},m}$  respectively denote constant and traffic-dependent power consumption of the fronthaul link connected to  $m$ th AP. Similarly,  $P_{c,a}$  and  $P_{\text{bh},a}$  respectively represent constant and traffic-dependent power consumption of the backhaul

link connected to  $a$ th AN. Furthermore,  $R_{u,m}$  and  $R_{u,a}$  are total uplink data rates transferred through  $m$ th AP and  $a$ th AN, respectively. To present Fig. 4(e), the UE's transmission power is swiped from 1 [ $\mu$ Watt] to 100 [Watt]. According to the increasing value of the network's power and the saturated value of the sum-SE at high transmission powers, the EE drops for an intense increase in the transmission power. In addition, from the sum-SE and EE perspectives, the UC-mMIMO approach provides better network performance than that of CF-mMIMO one thanks to the small amount of interference.

To exclusively evaluate the performance of the UC-mMIMO network, Fig. 4(f) depicts the CDF of the sum-SE under HI and clipping models and various amounts of served UEs by each AP, i.e.  $N_{UC}$ . It is represented that increasing numbers of  $N_{UC}$  decreases the sum-SE of the network. In other words, if the size of clustered UEs connected to APs degrades, the network's performance improves.

To study the effects of various numbers of UEs, APs, and ANs on the network's performance, Fig. 4(g) presents the sum-SE of the network as a function of the number of UEs  $K$  for the constant numbers of APs and ANs. Also, Fig. 4(h) represents the network's sum-SE versus the number of access points  $M$  for the fixed numbers of UEs and ANs, and Fig. 4(i) depicts the sum-SE of the network versus the number of aggregation nodes  $A$  for given numbers of UEs and APs. In all cases, by increasing the number of each parameter, the network's sum-SE continuously increases, and then its velocity shrinks for higher values. Thus, due to the presence of destructive impacts of the effective noise, the sum-SE increases slowly for higher numbers of  $K$ ,  $M$ , and  $A$ . In all figures, UCHI outperforms UCCL, CFHI, and CFCL. To depict the figures, the full-power transmissions and the unit gain coefficients are assumed for all scenarios.

The CDF of the network's sum-SE is presented in Fig. 5(a) for various scenarios and two classes of networks: Real and ideal networks. In the real network, we assume that the hardware models at APs and ANs are performed along with the impairment noises. Conversely, in the ideal network, we consider the perfect hardware. As expected, the ideal network outperforms the real one, and provides the upper bound. Furthermore, the UC-mMIMO network has better network performance than that of the CF-mMIMO one, and the HI model overcomes the clipping one. For all results, we assume full-power user data transmissions and unit gain coefficients.

To illustrate the effects of different weather conditions on the FSO-based fronthaul links and the network's performance, Fig. 5(b) and Fig. 5(c) respectively depict the CDFs for CF-mMIMO and UC-mMIMO networks under clear, rainy, snowy, and foggy weather states of

which the propagation coefficients are represented in Table II. It is presented that clear weather provides the best network performance, while foggy one has the worst performance. Moreover, for all weather conditions, UCHI overcomes other network scenarios. To represent this figure, the full-power transmissions and the unit gain coefficients are assumed for all scenarios.

## VII. CONCLUSION

We studied uplink data transmission of the CF- and the UC-mMIMO networks wherein the distributed APs are clustered and connected to serving ANs via FSO links, and the ANs communicate with the CPU over optical fiber backhubs. All APs and ANs convert their received signals to be well-matched to the optical links and transmit them to the other end. After acquiring the channel state information at the CPU from the transmitted channel training by the users, by applying the MRC and UatF techniques at the CPU, the uplink achievable data rates were derived for both CF- and UC-mMIMO scenarios, by taking into account the effects of HI and clipping models at APs and ANs. Then, we formulated the optimization problem to maximize the sum-rate of the network subject to maximum transmit power of the users, APs and the ANs. Optimal resource allocations are derived by transforming the non-convex optimization problem to the convex one to be solved by the geometric programming. Finally, the network's sum energy- and spectral-efficiency were investigated through numerical results to compare various network scenarios and underscore the performance characteristic of the network. It was concluded that the UC-mMIMO outperforms the CF-mMIMO one, and the HI model exceeds the clipping model.

## APPENDIX A

### SINR DERIVATION

To derive the SINR, after a sequence of mathematical manipulations, in the following, we derive the variance of each term given in (34).

#### A. $DS_k$

Since the channel coefficients are i.i.d., we have

$$\begin{aligned} DS_k &= \sqrt{\rho_u \eta_k} \sum_{a=1}^A \sum_{m \in \mathcal{M}(a)} A_{am} \Gamma_{am} \mathbb{E} \{g_{mk} \tilde{g}_{mk}^{a*}\} \\ &= \sqrt{\rho_u \eta_k} \sum_{a=1}^A \sum_{m \in \mathcal{M}(a)} A_{am} \Gamma_{am} \mathbb{E} \{(\tilde{g}_{mk}^{a*} + e_{mk}^a) \tilde{g}_{mk}^{a*}\} \end{aligned}$$

$$= \sqrt{\rho_u \eta_k} \sum_{a=1}^A \sum_{m \in \mathcal{M}(a)} A_{am} \Gamma_{am} \gamma_{mk}^a, \quad (47)$$

where  $e_{mk}^a = g_{mk} - \tilde{g}_{mk}^{a*}$  denotes the estimation error modeled as a zero-mean Gaussian random variable with the variance of  $\beta_{mk} - \gamma_{mk}^a$ , where  $e_{mk}^a$  and  $\tilde{g}_{mk}^{a*}$  are independent.

B.  $\mathbb{E}\{|\text{BU}_k|^2\}$

As the variance of a sum of independent random variables is equal to the sum of the variances, we have

$$\begin{aligned} \mathbb{E}\{|\text{BU}_k|^2\} &= \rho_u \eta_k \mathbb{E}\left\{\left|\sum_{a=1}^A \sum_{m \in \mathcal{M}(a)} A_{am} h_{am} g_{mk} \tilde{g}_{mk}^{a*} \mathbb{E}\left\{\sum_{a=1}^A \sum_{m \in \mathcal{M}(a)} A_{am} h_{am} g_{mk} \tilde{g}_{mk}^{a*}\right\}\right|^2\right\} \\ &= \rho_u \eta_k \sum_{a=1}^A \sum_{m \in \mathcal{M}(a)} A_{am}^2 \left(\Gamma_{am}^2 \mathbb{E}\{|g_{mk} \tilde{g}_{mk}^{a*}|^2\} - (\Gamma_{am})^2 |\mathbb{E}\{g_{mk} \tilde{g}_{mk}^{a*}\}|^2\right) \\ &= \rho_u \eta_k \sum_{a=1}^A \sum_{m \in \mathcal{M}(a)} A_{am}^2 \left(\Gamma_{am}^2 \beta_{mk} + (\Gamma_{am}^2 - (\Gamma_{am})^2) \gamma_{mk}^a\right) \gamma_{mk}^a. \end{aligned} \quad (48)$$

C.  $\mathbb{E}\{|\text{IUI}_{kk'}|^2\}$

Since the pilot sequences are mutually orthogonal, we have

$$\begin{aligned} \mathbb{E}\{|\text{IUI}_{kk'}|^2\} &= \rho_u \eta_{k'} \mathbb{E}\left\{\left|\sum_{a=1}^A \sum_{m \in \mathcal{M}(a)} A_{am} h_{am} g_{mk'} \tilde{g}_{mk}^{a*}\right|^2\right\} \\ &= \rho_u \eta_{k'} \mathbb{E}\left\{\left|\sum_{a=1}^A \sum_{m \in \mathcal{M}(a)} A_{am} h_{am} g_{mk'} \zeta_{mk}^a \right.\right. \\ &\quad \times \left.\left(\sqrt{\tau_p \rho_p} A_{am} h_{am} \sum_{k''=1}^K g_{mk''} \varphi_k^H \varphi_{k''} + n_{p,amk}^{\text{all}}\right)^*\right|^2\Big\} \\ &= \tau_p \rho_p \rho_u \eta_{k'} \mathbb{E}\left\{\left|\sum_{a=1}^A \sum_{m \in \mathcal{M}(a)} A_{am}^2 h_{am}^2 g_{mk'} \zeta_{mk}^a \left(\sum_{k''=1}^K g_{mk''} \varphi_k^H \varphi_{k''}\right)^*\right|^2\right\} \\ &\quad + \rho_u \eta_{k'} \mathbb{E}\left\{\left|\sum_{a=1}^A \sum_{m \in \mathcal{M}(a)} A_{am} h_{am} g_{mk'} \zeta_{mk}^a (n_{p,amk}^{\text{all}})^*\right|^2\right\} \\ &= \rho_u \eta_{k'} \sum_{a=1}^A \sum_{m \in \mathcal{M}(a)} A_{am}^2 \frac{\Gamma_{am}^4}{(\Gamma_{am})^2} \frac{\beta_{mk'}}{\beta_{mk}} (\gamma_{mk}^a)^2 \\ &\quad + \rho_u \eta_{k'} \sum_{a=1}^A \sum_{m \in \mathcal{M}(a)} A_{am}^2 \Gamma_{am}^2 \beta_{mk'} (\zeta_{mk}^a)^2 \Omega_{p,amk}^2 \end{aligned}$$

$$= \rho_u \eta_{k'} \sum_{a=1}^A \sum_{m \in \mathcal{M}(a)} A_{am}^2 \beta_{mk'} \left( \frac{\Gamma_{am}^4 (\gamma_{mk}^a)^2}{(\Gamma_{am})^2 \beta_{mk}} \Gamma_{am}^2 (\zeta_{mk}^a)^2 \Omega_{p,amk}^2 \right). \quad (49)$$

D.  $\mathbb{E}\{|N_k|^2\}$

It can be shown that the overall additive noise is uncorrelated with the channel coefficients. Thus, we have

$$\begin{aligned} \mathbb{E}\{|N_k|^2\} &= \mathbb{E}\left\{\left|\sum_{a=1}^A \sum_{m \in \mathcal{M}(a)} n_{u,am}^{all} \tilde{g}_{mk}^{a*}\right|^2\right\} \\ &= \sum_{a=1}^A \sum_{m \in \mathcal{M}(a)} \gamma_{mk}^a \Omega_{u,am}^2. \end{aligned} \quad (50)$$

By plugging (47), (48), (49), and (50) into (34), (35) is obtained.

## REFERENCES

- [1] T. L. Marzetta, “Noncooperative cellular wireless with unlimited numbers of base station antennas,” *IEEE Transactions on Wireless Communications*, vol. 9, no. 11, pp. 3590–3600, 2010.
- [2] —, *Fundamentals of massive MIMO*. Cambridge University Press, 2016.
- [3] M. N. Khormuji, “Generalized semi-orthogonal multiple-access for massive MIMO,” in *IEEE 81st Vehicular Technology Conference (VTC Spring)*, pp. 1–5, 2015.
- [4] H. Q. Ngo, A. Ashikhmin, H. Yang, E. G. Larsson, and T. L. Marzetta, “Cell-free massive MIMO versus small cells,” *IEEE Transactions on Wireless Communications*, vol. 16, no. 3, pp. 1834–1850, 2017.
- [5] A. Kabiri, M. J. Emadi, and M. N. Khormuji, “Optimal design of semi-orthogonal multiple-access massive MIMO systems,” *IEEE Communications Letters*, vol. 21, no. 10, pp. 2230–2233, 2017.
- [6] T. C. Mai, H. Q. Ngo, M. Egan, and T. Q. Duong, “Pilot power control for cell-free massive MIMO,” *IEEE Transactions on Vehicular Technology*, vol. 67, no. 11, pp. 11 264–11 268, 2018.
- [7] S. Buzzi and C. D’Andrea, “Cell-free massive MIMO: User-centric approach,” *IEEE Wireless Communications Letters*, vol. 6, no. 6, pp. 706–709, 2017.
- [8] S. Buzzi and C. D’Andrea, “User-centric communications versus cell-free massive MIMO for 5G cellular networks,” in *21th International ITG Workshop on Smart Antennas (WSA)*, pp. 1–6, 2017.
- [9] S. Buzzi, C. D’Andrea, A. Zappone, and C. D’Elia, “User-centric 5G cellular networks: Resource allocation and comparison with the cell-free massive MIMO approach,” *IEEE Transactions on Wireless Communications*, 2019.
- [10] H. Q. Ngo, L.-N. Tran, T. Q. Duong, M. Matthaiou, and E. G. Larsson, “On the total energy efficiency of cell-free massive MIMO,” *IEEE Transactions on Green Communications and Networking*, vol. 2, no. 1, pp. 25–39, 2017.
- [11] H. Yang and T. L. Marzetta, “Energy efficiency of massive MIMO: Cell-free vs. cellular,” in *IEEE 87th Vehicular Technology Conference (VTC Spring)*, pp. 1–5, 2018.
- [12] H. Masoumi and M. J. Emadi, “Performance analysis of cell-free massive mimo system with limited fronthaul capacity and hardware impairments,” *IEEE Transactions on Wireless Communications*, vol. 19, no. 2, pp. 1038–1053, 2019.

- [13] M. Bashar, K. Cumanan, A. G. Burr, H. Q. Ngo, M. Debbah, and P. Xiao, "Max-min rate of cell-free massive MIMO uplink with optimal uniform quantization," *IEEE Transactions on Communications*, vol. 67, no. 10, pp. 6796–6815, 2019.
- [14] M. Z. Hassan, M. J. Hossain, J. Cheng, and V. C. Leung, "Statistical delay-QoS aware joint power allocation and relaying link selection for free space optics based fronthaul networks," *IEEE Transactions on Communications*, vol. 66, no. 3, pp. 1124–1138, 2017.
- [15] M. A. Khalighi and M. Uysal, "Survey on free space optical communication: A communication theory perspective," *IEEE Communications Surveys & Tutorials*, vol. 16, no. 4, pp. 2231–2258, 2014.
- [16] H. Kaushal and G. Kaddoum, "Optical communication in space: Challenges and mitigation techniques," *IEEE Communications Surveys & Tutorials*, vol. 19, no. 1, pp. 57–96, 2016.
- [17] A. Douik, H. Dahrouj, T. Y. Al-Naffouri, and M.-S. Alouini, "Hybrid radio/free-space optical design for next generation backhaul systems," *IEEE Transactions on Communications*, vol. 64, no. 6, pp. 2563–2577, 2016.
- [18] A. Touati, A. Abdaoui, F. Touati, M. Uysal, and A. Bouallegue, "On the effects of combined atmospheric fading and misalignment on the hybrid FSO/RF transmission," *Journal of Optical Communications and Networking*, vol. 8, no. 10, pp. 715–725, 2016.
- [19] L. Chen, W. Wang, and C. Zhang, "Multiuser diversity over parallel and hybrid FSO/RF links and its performance analysis," *IEEE Photonics Journal*, vol. 8, no. 3, pp. 1–9, 2016.
- [20] M. Usman, H.-C. Yang, and M.-S. Alouini, "Practical switching-based hybrid FSO/RF transmission and its performance analysis," *IEEE Photonics Journal*, vol. 6, no. 5, pp. 1–13, 2014.
- [21] W. Zhang, S. Hranilovic, and C. Shi, "Soft-switching hybrid FSO/RF links using short-length raptor codes: Design and implementation," *IEEE Journal on Selected Areas in Communications*, vol. 27, no. 9, pp. 1698–1708, 2009.
- [22] V. Jamali, D. S. Michalopoulos, M. Uysal, and R. Schober, "Link allocation for multiuser systems with hybrid RF/FSO backhaul: Delay-limited and delay-tolerant designs," *IEEE Transactions on Wireless Communications*, vol. 15, no. 5, pp. 3281–3295, 2016.
- [23] M. Najafi, V. Jamali, and R. Schober, "Optimal relay selection for the parallel hybrid RF/FSO relay channel: Non-buffer-aided and buffer-aided designs," *IEEE Transactions on Communications*, vol. 65, no. 7, pp. 2794–2810, 2017.
- [24] K. Ahmed and S. Hranilovic, "C-RAN uplink optimization using mixed radio and FSO fronthaul," *IEEE/OSA Journal of Optical Communications and Networking*, vol. 10, no. 6, pp. 603–612, 2018.
- [25] M. Najafi, V. Jamali, D. W. K. Ng, and R. Schober, "C-RAN with hybrid RF/FSO fronthaul links: Joint optimization of RF time allocation and fronthaul compression," in *IEEE Global Communications Conference (GLOBECOM)*, pp. 1–7, 2017.
- [26] M. Z. Hassan, M. J. Hossain, J. Cheng, and V. C. Leung, "Joint FSO fronthaul and millimeter-wave access link optimization in cloud small cell networks: A statistical-QoS aware approach," *IEEE Transactions on Communications*, vol. 67, no. 6, pp. 4208–4226, 2019.
- [27] X.-H. Huang, H.-H. Lu, S. Donati, C.-Y. Li, Y.-C. Wang, Y.-B. Jheng, and J.-C. Chang, "Two-way wireless-over-fibre and FSO-over-fibre communication systems with an optical carrier transmission," *Laser Physics*, vol. 28, no. 7, p. 076207, 2018.
- [28] X.-H. Huang, H.-H. Lu, C.-Y. Li, Y.-C. Wang, J.-C. Chang, Y.-B. Jheng, and W.-S. Tsai, "Fiber-FSO/wireless convergent systems based on dual-polarization and one optical sideband transmission schemes," *Laser Physics*, vol. 28, no. 6, p. 066205, 2018.
- [29] C.-H. Yeh, C.-S. Gu, B.-S. Guo, Y.-J. Chang, C.-W. Chow, M.-C. Tseng, and R.-B. Chen, "Hybrid free space optical communication system and passive optical network with high splitting ratio for broadcasting data traffic," *Journal of Optics*, vol. 20, no. 12, p. 125702, 2018.

- [30] A. E. Morra, K. Ahmed, and S. Hranilovic, "Impact of fiber nonlinearity on 5G backhauling via mixed FSO/fiber network," *IEEE Access*, vol. 5, pp. 19 942–19 950, 2017.
- [31] A. E. Morra and S. Hranilovic, "Mixed mmWave and radio-over-fiber systems with fiber nonlinearity," *IEEE Photonics Technology Letters*, vol. 31, no. 1, pp. 23–26, 2018.
- [32] R. C. Kizilirmak, O. Narmanlioglu, and M. Uysal, "Centralized light access network (C-LiAN): A novel paradigm for next generation indoor VLC networks," *IEEE Access*, vol. 5, pp. 19 703–19 710, 2017.
- [33] J. Beysens, A. Galisteo, Q. Wang, D. Juara, D. Giustiniano, and S. Pollin, "DenseVLC: A cell-free massive MIMO system with distributed LEDs," in *14th International Conference on emerging Networking EXperiments and Technologies*, pp. 320–332, 2018.
- [34] I. S. Ansari, F. Yilmaz, and M.-S. Alouini, "Impact of pointing errors on the performance of mixed RF/FSO dual-hop transmission systems," *IEEE Wireless Communications Letters*, vol. 2, no. 3, pp. 351–354, 2013.
- [35] S. Anees and M. R. Bhatnagar, "Performance of an amplify-and-forward dual-hop asymmetric RF–FSO communication system," *Journal of Optical Communications and Networking*, vol. 7, no. 2, pp. 124–135, 2015.
- [36] M. I. Petkovic, A. M. Cvetkovic, G. T. Djordjevic, and G. K. Karagiannidis, "Outage performance of the mixed RF/FSO relaying channel in the presence of interference," *Wireless Personal Communications*, vol. 96, no. 2, pp. 2999–3014, 2017.
- [37] E. Soleimani-Nasab and M. Uysal, "Generalized performance analysis of mixed RF/FSO cooperative systems," *IEEE Transactions on Wireless Communications*, vol. 15, no. 1, pp. 714–727, 2015.
- [38] C. Studer, M. Wenk, and A. Burg, "MIMO transmission with residual transmit-RF impairments," in *IEEE International ITG workshop on smart antennas (WSA)*, pp. 189–196, 2010.
- [39] U. Gustavsson, C. Sánchez-Perez, T. Eriksson, F. Athley, G. Durisi, P. Landin, K. Hausmair, C. Fager, and L. Svensson, "On the impact of hardware impairments on massive MIMO," in *IEEE Globecom Workshops (GC Wkshps)*, pp. 294–300, 2014.
- [40] S. Jacobsson, U. Gustavsson, G. Durisi, and C. Studer, "Massive MU-MIMO-OFDM uplink with hardware impairments: Modeling and analysis," in *IEEE Asilomar Conference on Signals, Systems, and Computers*, pp. 1829–1835, 2018.
- [41] E. Björnson, J. Hoydis, M. Kountouris, and M. Debbah, "Massive MIMO systems with non-ideal hardware: Energy efficiency, estimation, and capacity limits," *IEEE Transactions on Information Theory*, vol. 60, no. 11, pp. 7112–7139, 2014.
- [42] J. Zhang, Y. Wei, E. Björnson, Y. Han, and S. Jin, "Performance analysis and power control of cell-free massive MIMO systems with hardware impairments," *IEEE Access*, vol. 6, pp. 55 302–55 314, 2018.
- [43] E. Björnson, M. Matthaiou, and M. Debbah, "Massive MIMO with non-ideal arbitrary arrays: Hardware scaling laws and circuit-aware design," *IEEE Transactions on Wireless Communications*, vol. 14, no. 8, pp. 4353–4368, 2015.
- [44] J. Zhang, X. Xue, E. Björnson, B. Ai, and S. Jin, "Spectral efficiency of multipair massive MIMO two-way relaying with hardware impairments," *IEEE Wireless Communications Letters*, vol. 7, no. 1, pp. 14–17, 2017.
- [45] A. M. Abdalla, J. Rodriguez, I. Elfergani, and A. Teixeira, *Optical and Wireless Convergence for 5G Networks*. Wiley Online Library, 2020.
- [46] M. A. Saeidi, M. J. Emadi, H. Masoumi, M. R. Mili, D. W. K. Ng, and I. Krikidis, "Weighted sum-rate maximization for multi-IRS-assisted full-duplex systems with hardware impairments," *arXiv preprint arXiv:2010.01339*, 2020.